



# Experimental Study of the Performance of the Air-Based Standing Wave Thermoacoustic Refrigerator Using Parallel Wave Stack

Praitoon Chaiwongsa<sup>1</sup> · Somchai Wongwises<sup>1,2</sup>

Received: 24 April 2022 / Accepted: 5 July 2022 / Published online: 10 August 2022

© The Author(s), under exclusive licence to Springer Science+Business Media, LLC, part of Springer Nature 2022

## Abstract

The novelty of this work is a new type of stack, namely, the parallel wave stack (PWS). In this paper, we study the performance of an air-based standing wave thermoacoustic refrigerator using the PWS. We use small heat pipes with a heat transfer rate of approximately 30 W as heat exchangers for the system. We investigate the effect of the ratio of stack length ( $L_s$ ) to the distance between stack center and reflector ( $X_s$ ) on the performance of the refrigerator parallel wave stacks with a blockage ratio (BR) of 67 %, 71 %, and 74 %, and with  $L_s/X_s$  ratios of 0.74, 0.96, and 1.20. We tested and compared these under a cooling load ( $Q_c$ ) of 0.5 W to 2 W and a frequency of 150 Hz. The results show that a BR of 71% with an  $L_s/X_s$  ratio of 0.96 provides a minimum cold-side temperature ( $T_c$ ), and a maximum temperature difference ( $\Delta T_m$ ), a maximum coefficient of performance, and a maximum relative coefficient of performance. This new type of stack can provide a higher performance. The structure of the stack is also stronger than others. This stack is an alternative and can be used in a thermoacoustic refrigerator. The results obtained from the present study will be very useful for improving the performance of the thermoacoustic refrigerator in the future.

**Keywords** Blockage ratio · Coefficient of performance · Parallel wave stack · Small heat pipes · Thermoacoustic refrigerator

## Nomenclature

$A_s$  Heat transfer area ( $m^2$ )  
PWS Parallel wave stack

---

✉ Somchai Wongwises  
somchai.won@kmutt.ac.th

<sup>1</sup> Fluid Mechanics, Thermal Engineering and Multiphase Flow Research Lab. (FUTURE), Department of Mechanical Engineering, Faculty of Engineering, King Mongkut's University of Technology Thonburi, Bangmod, Bangkok 10140, Thailand

<sup>2</sup> National Science and Technology Development Agency (NSTDA), Pathum Thani 12120, Thailand

BR	Blockage ratio (%)
$Q_c$	Cooling load (W)
COP	Coefficient of performance
TAR	Thermoacoustic refrigerator
COP <sub>c</sub>	Carnot coefficient of performance
$T_c$	Cold-side temperature (°C)
COPR	Relative coefficient of performance
$T_h$	Hot-side temperature (°C)
$E_i$	Electrical input voltage (V)
$X_s$	Distance between stack center and reflector (m)
$f$	Frequency (Hz)
$I_i$	Electrical input current (A)
$L_s$	Stack length (m)
$\rho_m$	Mean density ( $\text{kg}\cdot\text{m}^{-3}$ )
$P_i$	Electrical input power (W)
$\Delta T_m$	Temperature difference (°C)

## 1 Introduction

A thermoacoustic refrigerator (TAR) is an example of thermoacoustic technology, which is a clean technology. The TAR uses acoustic energy to pump and reject heat in the system. Operating gases used in TARs are not toxic, but environmentally friendly, causing no problems to the environment. This is different from conventional refrigerators, which use refrigerants that destroy the ozone and cause global warming. In addition, there are no moving parts that make the TAR superior to conventional refrigerators.

Rott [1] presented a theory of thermoacoustics for heating and refrigeration. Hoffer [2] constructed the first standing wave thermoacoustic refrigerator (SWTAR) prototype using Rott's approach. The SWTAR was created with the highest relative coefficient of performance (COPR) at 12.6 %. Swift [3] wrote an article covering the critical aspects of the thermoacoustic engine and its applications.

Garrett et al. [4] constructed and tested a small TAR. Their TAR had a drive ratio of 2 % and was filled with a 150 psia mixture of He (97.20 %) and Xe (2.70 %). It was found that the COPR of the system was higher than 16 %. Swift [5] presented the fundamental of thermoacoustics and its application in the commercial market. Wetzel and Herman [6] improved an algorithm to determine the performance of TAR. They used an algorithm to predict COPR with a thermoacoustic effect of about 40 % to 50 %.

Belcher et al. [7] analyzed the properties of noble gases with various mixtures for driving thermoacoustic engines. Poese and Garrett [8] compared measured data and a linear model. The deviation of heat pump power was about 23 %. Tijani et al. [9, 10] presented the component design of a TAR [10] at high amplitude that was similar to the methods of Wetzel and Herman [6]. They also described the construction of a small SWTAR [9]. However, its resonator was modified

to reduce acoustic power loss. The lowest temperature of the TAR designed by Tijani et al. [10] was  $-65\text{ }^{\circ}\text{C}$  with a cooling power of 4 W.

Herman and Chen [11] developed a model to analyze the heat transfer rate in a TAR. The results showed that the heat exchanger's Peclet number and heat transfer from the working gas had a significant impact on the refrigerating process and the outlet temperature of the working fluid. Akhavanbazaz et al. [12] studied the effect of gas blockage in the heat exchangers. The results indicated that the larger the area of the heat exchanger, the higher the heat transfer rate and the lower the cooling power. In these conditions, the acoustic power of the system increased due to a higher gas blockage. Nsofor and Ali [13] designed a TAR that was similar to Tijani's prototype [9]. This TAR system used helium at a pressure of 3–6 bars, a frequency of 250 Hz to 500 Hz, and a cooling load of 1 W to 4 W. The results showed that the higher cooling load and the higher temperature difference ( $\Delta T_m$ ) did not depend only on the high pressure of the system but also on the optimum frequency of the system.

Tasnim et al. [14] developed a model to investigate the effect of thermoacoustic fluid and operating conditions on the performance of a TAR. The results showed that the performance of a TAR could not be improved by a working gas at a low Prandtl number. They compared the results with experimental data and found it to be consistent. Nayak et al. [15] studied the effect of the geometrical shape and material of the stack on the performance of an SWTAR. They tested and compared four geometrical shapes and three types of materials of the stack. They found that at cooling loads of 2 W and a frequency of 400 Hz, the  $\Delta T_m$  was the highest. At 10 bars, the  $\Delta T_m$  was  $19.4\text{ }^{\circ}\text{C}$  for a mylar parallel plate stack. This  $\Delta T_m$  was more than that obtained from other geometries. Yahya et al. [16] experimented with three types of stacks to study the performance of an air-based standing wave thermoacoustic refrigerator (ASWTAR). The results indicated that the best stack type was a mylar parallel plate stack. The COP and COPR of the system were 0.217, and 0.0015, respectively, for mylar-plate stacks.

Wantha [17] tested a TAR with three different stack geometries to analyze the cold-side temperature of the stack that they received and that was influenced by mean pressure in the system. The results indicated that the average pressure in the system had a significant effect on cold-side temperature. Chaiwongsa and Wongwises [18] studied and tested the performance of an ASWTAR using a spiral stack with a blockage ratio (BR) of about 0.62. Small heat pipes were used for the cold-side and hot-side heat exchangers of the refrigerator. The results indicated that the slope of the COP decreased as acoustic power increased.

Chaiwongsa and Wongwises [19] investigated the effect of the stack geometry on the performance of an ASWTAR. A circular stack made from polylactic acid (PLA) with three sizes of blockage ratio and one size of a spiral stack made from Mylar was tested and compared. They tested the system performance at a frequency of 150 Hz with a cooling load ( $Q_c$ ) of 0.5 W to 2 W. The results showed that a circular stack with a BR of 71 % provided a minimum cold-side temperature. Additionally, all three sizes of a circular stack provided higher  $\Delta T_m$ , COP, and COPR than a spiral stack. This indicated that the property of materials directly affected the performance of the system.

As described above, a number of researchers have researched the thermoacoustic refrigerator, both experimentally and analytically. However, it should be noted that the studies found in the literature described above focused on the spiral stack and parallel plates stack. The parallel wave stack (PWS), which is the innovation of the present study, remains unstudied. Moreover, the effect of stack length ( $L_s$ ) and distance between stack center and reflector ( $X_s$ ) on the COP of ASWTAR has received comparatively little attention in the literature. To the best of our knowledge, there has been only one work, that of Tijani et al. (2002), dealing with this issue. However, they presented only the numerical results obtained from the parallel flat stack (PFS). In the present study, we aim to present a new type of stack—the parallel wave stack (PWS). Three different ratios of stack length to distance between stack center and reflector ( $L_s/X_s$ ) are used in the experiment. Small heat pipes are used as the cold-side and the hot-side heat exchangers in an ASWTAR. Both heat exchangers are easy to install. The structure is not complicated and provides small flow obstruction. Additionally, the material used for PWS in this investigation is polylactic acid (PLA), which has better thermal properties than the materials applied in the previous studies. The performance of a refrigerator using PWS has never before appeared in the literature.

## 2 Experimental Setup and Procedure

The experimental apparatus, measuring instruments, experimental procedure, and data reduction are the same as those described by Chaiwongsa and Wongwiset [19]. The only difference is in the test section.

Figure 1 shows the geometry of a PWS made with polylactic acid through 3D printing. We tested and compared a parallel wave stack with blockage ratios (BR) of 67 %, 71 %, and 74 %, and ratios of stack length ( $L_s$ ) to a distance between stack center and reflector ( $X_s$ ) of 0.74, 0.96, and 1.20. The  $L_s/X_s$  ratios used in this study

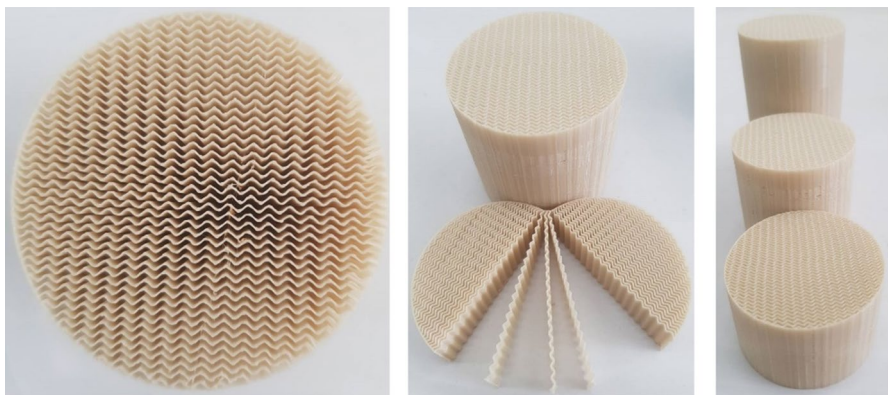


Fig. 1 Parallel Wave Stack (PWS)

are 0.74, 0.96, and 1.20 for an  $L_s$  of 35 mm, 55 mm, and 90 mm, respectively, as shown in Table 1.

We performed the first tests to determine the resonant frequency of the system. The tests were performed at an  $L_s/X_s$  ratio of 0.96 and BR of 67 %, 71 %, and 74 % without a cooling load at a frequency of 120 Hz to 190 Hz and an input power of 20 W. The last tests were performed to evaluate the performance of an ASWTAR in terms of  $T_c$ ,  $\Delta T_m$ , COP, and COPR. We tested and compared the  $L_s/X_s$  ratios of 0.74, 0.96, and 1.20 with optimum blockage ratios obtained from the first tests, under a cooling load of 0.5 W to 2 W and a resonant frequency.

### 3 Results and Discussion

#### 3.1 Optimum Operating Conditions

Figure 2 shows the variation of the electrical input voltage ( $E_i$ ) and the electrical input current ( $I_i$ ) along with the operating frequency ( $f$ ) for the BR of 67 %, 71 %, and 74 %, under an input power ( $P_i$ ) of 20 W. The figure shows that in the first period, the  $E_i$  will rise when the frequency rises. The  $E_i$  rises to the maximum value when the frequency is 150 Hz, and then decreases as the frequency rises. In contrast, when the frequency rises, the  $I_i$  will decrease. At 150 Hz, the  $I_i$  decreases to a minimum, and after that, it will start to rise as the frequency rises. Comparing the  $E_i$  at three different sizes of the BR, it is clear that the highest  $E_i$  is the same for all three sizes of the BR. Likewise, when comparing the  $I_i$  at three sizes of the BR, it is evident that a BR of 67 %, 71 %, and 74 % gives the same lowest  $I_i$ . This is because when a thermoacoustic effect occurs, the resistance of the working gas decreases, and the electrical resistance in the voice coil of the driver increases accordingly. An

**Table 1** Design parameters

	Symbol	Value			Unit
<b>Parameters</b>					
Stack length	$L_s$	35	55	90	mm
Distance between stack center and reflector	$X_s$	47.5	57.5	75.0	mm
Stack thickness	$2l_0$		0.25		mm
Stack spacing	$2y_0$		0.7		mm
Ratio of stack length to distance between stack center and reflector	$L_s/X_s$	0.74	0.96	1.20	–
Thermal penetration depth	$\delta_k$		0.217		mm
Blockage ratio	BR		71		%
Heat transfer area	$A_s$	0.20	0.31	0.51	m <sup>2</sup>
<b>Properties of PLA</b>					
Density	$\rho_s$		1300		kg·m <sup>-3</sup>
Thermal conductivity	$k_s$		0.13		W·m <sup>-1</sup> ·K <sup>-1</sup>
Specific heat	$c_s$		1800		J·kg <sup>-1</sup> ·K <sup>-1</sup>

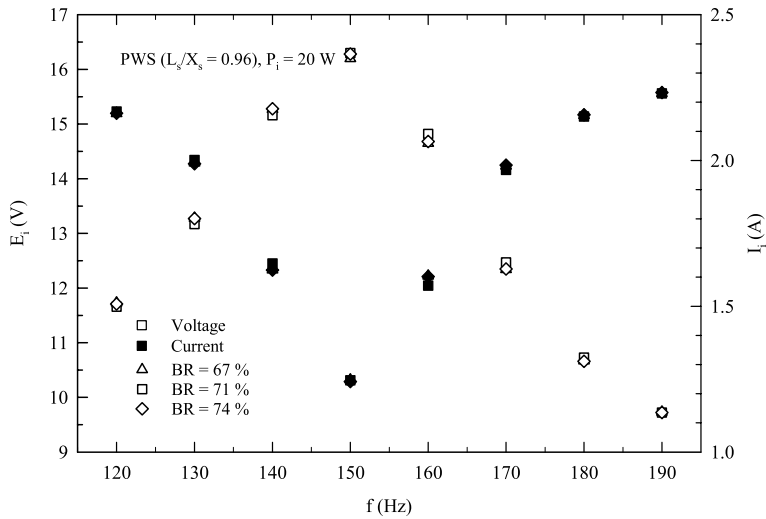


**Fig. 2** Relationship of  $E_i$  and  $I_i$  along with the frequency for three size blockage ratios at an input power of 20 W

increase in the resistance also decreases the  $I_i$ , resulting in an increase in  $E_i$  [18]. Moreover, we can confirm that the resonant frequency is 150 Hz, which is the best operating frequency for the system.

Figure 3 shows the variation of the  $T_c$  with an operating frequency for the BR of 67 %, 71 %, and 74 % under a  $P_i$  of 20 W. The figure shows that the  $T_c$  decreases to a minimum at 150 Hz, and then rises as the frequency rises. When the system

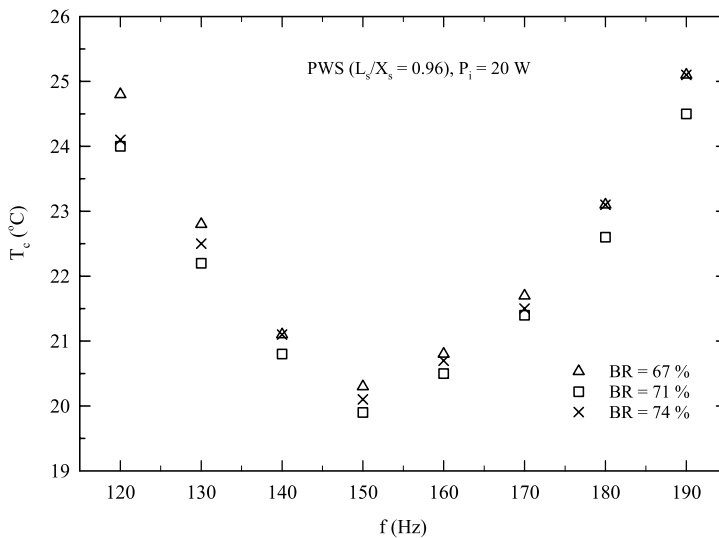


**Fig. 3** Relationship of  $T_c$  and frequency for three size blockage ratios at an input power of 20 W

is operating under optimal conditions, the thermoacoustic effect will increase, heat pumping in the process and then heat transfer in the stack will also increase. Therefore, the  $T_c$  at a frequency of 150 Hz is lower than the  $T_c$  at other frequencies. When comparing the  $T_c$  at all three sizes of the BR, the figure shows that the minimum  $T_c$  for the BR of 71 %, 74 %, and 67 %, are 19.9 °C, 20.1 °C, and 20.3 °C, respectively. It should be noted that among all minimum  $T_c$ ,  $T_c$  obtained from the system with the BR of 71 % is minimal, even though the heat transfer area is not maximum. This result reflects that the system with a BR of 71 % can absorb heat from the air better with less heat loss than other BR.

### 3.2 Cold-Side Temperature ( $T_c$ )

Figure 4 shows the variation of the  $T_c$  with a cooling load ( $Q_c$ ) for a BR of 71 % and the  $L_s/X_s$  ratios of 0.74, 0.96, and 1.20 under a frequency of 150 Hz. The graph shows that the  $T_c$  rises with a constant slope as the  $Q_c$  rises. It is to be noted that the  $T_c$  shown in the figure is the  $T_c$  obtained after applying acoustic power. While a certain cooling load is applied, the  $T_c$  will increase. To reduce the  $T_c$ , acoustic power has to be increased. However, the new  $T_c$  will not be lower than the original  $T_c$ . In the present study, an acoustic power used to form the heat transfer process in the stack is also small due to very low driver performance. Comparing  $T_c$  at various  $L_s/X_s$  ratios, the figure shows that, without a cooling load, the  $L_s/X_s$  ratio yielding the lowest, second lowest, and highest  $T_c$  are 0.96, 1.20, and 0.74, which yield a  $T_c$  of 20.3 °C, 21.8 °C, and 24.4 °C. For the maximum cooling load (2 W),  $T_c$  is 23.4 °C, 24.8 °C, and 29.2 °C for an  $L_s/X_s$  ratio of 0.96, 1.20, and 0.74 respectively.

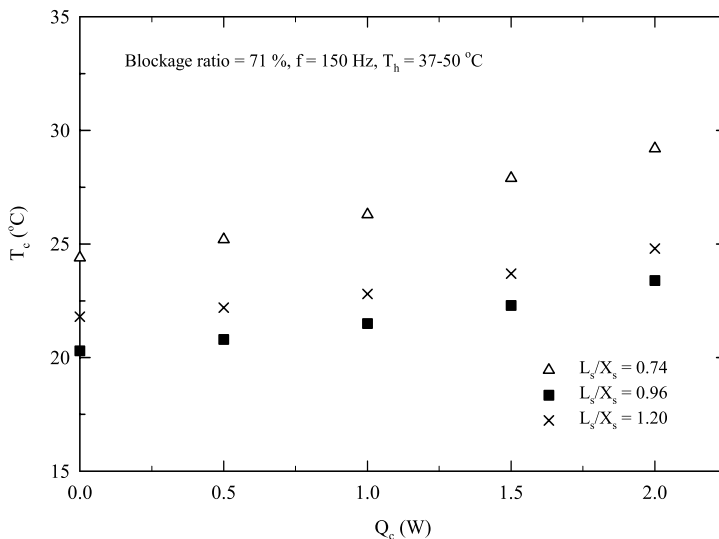


**Fig. 4** Relationship of  $T_c$  and  $Q_c$  for blockage ratios of 71 % with different  $L_s/X_s$  ratios at a frequency of 150 Hz

Additionally, when comparing the heat transfer surface area ( $A_s$ ) of the stack at various  $L_s/X_s$  ratios, we found that the  $L_s/X_s$  ratio with the highest to lowest  $A_s$  is 1.20 (0.59 m<sup>2</sup>), 0.96 (0.36 m<sup>2</sup>), and 0.74 (0.23 m<sup>2</sup>). It is worth noting that the  $L_s/X_s$  ratio of 0.96 yields lower  $T_c$  than other  $L_s/X_s$  ratios, although the  $A_s$  is not the highest. Having an optimal  $L_s/X_s$  ratio results in greater heat transfer from the cold side to the hot side of the stack. Therefore, the optimal  $L_s/X_s$  ratio for this study is 0.96, consistent with the results of the study by Tijani [9].

### 3.3 Temperature Difference ( $\Delta T_m$ )

Figure 5 shows the variation of the  $\Delta T_m$  with  $Q_c$  for the BR of 71 % and an  $L_s/X_s$  ratio of 0.74, 0.96, and 1.20 under a frequency of 150 Hz. It is to be noted that  $\Delta T_m$  can be calculated from the equation  $\Delta T_m = T_h - T_c$ , where  $T_h$  is the hot-side temperature. The graph shows that the increase in  $Q_c$  tends to change  $\Delta T_m$  in two cases. For the  $L_s/X_s$  ratio of 0.96 and 1.20, when  $Q_c$  increases,  $\Delta T_m$  tends to increase. While the  $L_s/X_s$  ratio is at 0.74, as  $Q_c$  increases  $\Delta T_m$  tends to decrease. When comparing  $\Delta T_m$  at various  $L_s/X_s$  ratios, the graph indicates that, without cooling load, the  $L_s/X_s$  ratio with the highest and lowest  $\Delta T_m$  are 0.96 (24.1 °C) and 0.74 (13.0 °C). For the maximum cooling load (2 W), the  $L_s/X_s$  ratio with the highest  $\Delta T_m$  is 0.96 (26.9 °C) and the lowest  $\Delta T_m$  is 0.74 (11.0 °C). The system can increase the heat transfer from the cold side to the hot side of the stack, thereby increasing the thermoacoustic effect of the system.

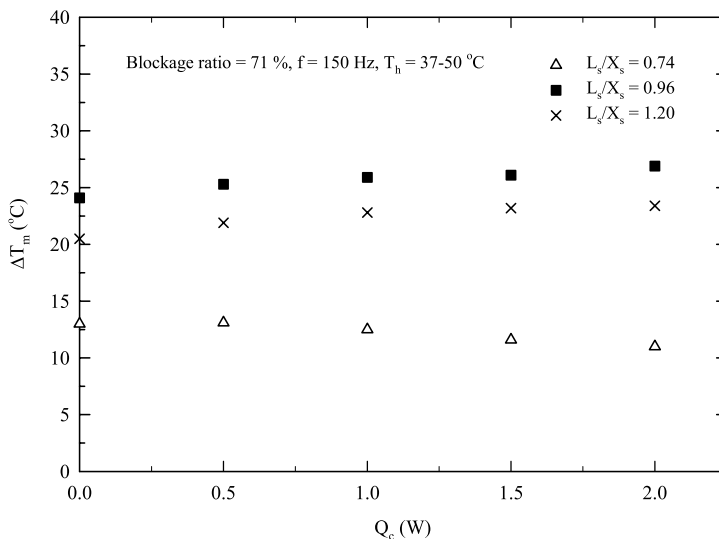


**Fig. 5** Relationship of  $\Delta T_m$  and  $Q_c$  for blockage ratios of 71 % with different  $L_s/X_s$  ratios at a frequency of 150 Hz



### 3.4 The COP of the System

Figure 6 shows the COP against  $Q_c$  for BR at 71 % with an  $L_s/X_s$  ratio of 0.74, 0.96, and 1.20 under a frequency of 150 Hz. The graph shows that COP increases with a nearly constant slope as  $Q_c$  increases. This is because the ratio of acoustic power, which is applied to the system until the cold-side temperature ( $T_c$ ) becomes constant, to  $Q_c$  is almost constant. The graph shows that at the same  $Q_c$ , all  $L_s/X_s$  ratios yielded almost the same COP. This is because, for each  $L_s/X_s$  ratio tested for a different  $Q_c$ , the acoustic power of the system changed very little. For the maximum cooling load (2 W), the COP for three sizes of  $L_s/X_s$  ratio is 3.31. As a result, we cannot determine the cause of the difference in the system's COP. Consequently, the COPR is the only indicator that can indicate that the performance of the system using different  $L_s/X_s$  ratios is different.

### 3.5 The COPc of the System

Figure 7 shows a Carnot coefficient of performance (COPc) of the system with a BR at 71 % and  $L_s/X_s$  ratio of 0.74, 0.96, and 1.20, plotted against  $Q_c$  under a frequency of 150 Hz. The COPc (or the theoretical COP) can be calculated from  $COPc = T_c/\Delta T_m$ . The graph indicates that the increase in  $Q_c$  tends to change COPc in two cases. For the  $L_s/X_s$  ratio of 0.96 and 1.20, when  $Q_c$  increases, the COPc tends to decrease. While the  $L_s/X_s$  ratio is 0.74, COPc tends to increase. It is worth noting that the COPc of a system using an  $L_s/X_s$  ratio of 0.74 is very high. However, if the system has an actual COP much lower than a COPc, the system should be

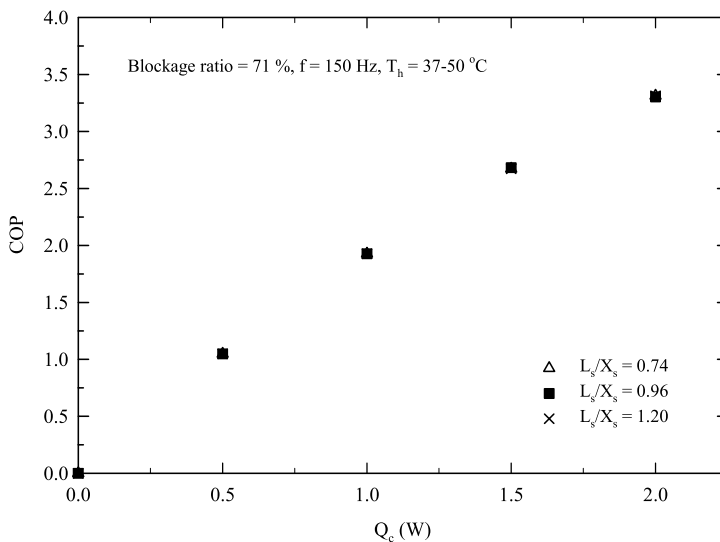


**Fig. 6** Relationship of COP and  $Q_c$  for blockage ratios of 71 % with different  $L_s/X_s$  ratios at a frequency of 150 Hz

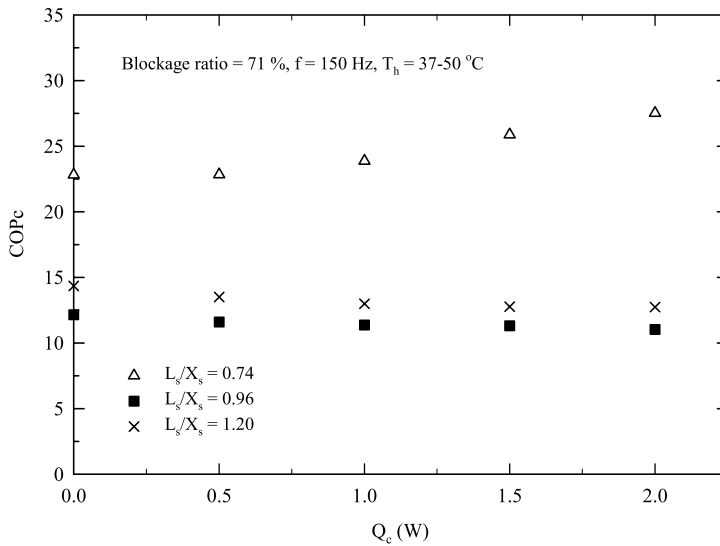


**Fig. 7** Relationship of COPc and  $Q_c$  for blockage ratios of 71 % with different  $L_s/X_s$  ratios at a frequency of 150 Hz

adjusted to achieve an actual COP closer to the COPc. Additionally, the graph shows that at the maximum cooling load (2 W), the  $L_s/X_s$  ratio yielding COPc from lowest to highest is 0.96 (11.03), 1.20 (12.74), and 0.74 (27.52).

### 3.6 The COPR of the System

Figure 8 shows the variation of COPR with  $Q_c$  for BR at 71 % and an  $L_s/X_s$  ratio of 0.74, 0.96, and 1.20 at 150 Hz. COPR is the ratio of actual COP and COPc. The figure shows that when  $Q_c$  increases, COPR increases. For the  $L_s/X_s$  ratio of 0.96 and 1.20, when  $Q_c$  increases, COPR decreases causing a large increase in COPR. For cases where the  $L_s/X_s$  ratio is 0.74, as  $Q_c$  increases, COPc also increases. However, increasing the COPc does not decrease COPR. The figure also shows that at different cooling loads, the  $L_s/X_s$  ratio providing maximum and minimum COPR values is 0.96 and 0.74. We can therefore conclude that the  $L_s/X_s$  ratio of 0.96 is the optimal ratio, at a cooling load of 2 W, and a maximum COPR of 29.9 %.

## 4 Conclusion

The parallel wave stack (PWS) is our innovation and has never before appeared in open literature. In the PWS, a corrugated, waveform surface provides the stack with a larger heat transfer area, resulting in a higher heat transfer rate between the air and the stack, in turn yielding a higher thermoacoustic effect. Moreover,

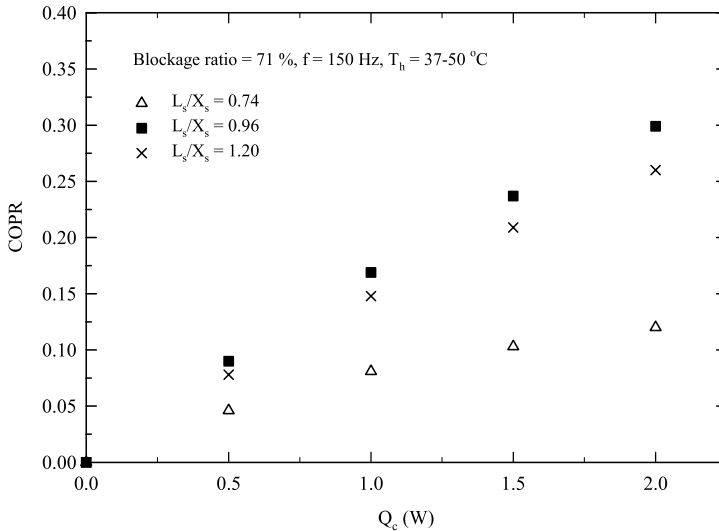


**Fig. 8** Comparison of COPR and  $Q_c$  for blockage ratios of 71 % with different  $L_s/X_s$  ratios at a frequency of 150 Hz

because our PWS has been fabricated from polylactic acid (PLA), which has a low thermal conductivity and a high specific heat, the thermoacoustic effect of the system is higher. The plate of the PWS with a corrugated surface will result in PWS being stronger than the parallel flat stack (PFS). Therefore, PWS is a new stack and an alternative for thermoacoustic devices that provides high performance, strength, and a longer service life. At present, with a 3D printer, stacks can be created with other special shapes as well as using non-air with other working fluids. The present results show that at a BR of 71 %, with an  $L_s/X_s$  ratio of 0.96, the system gives the lowest value of  $T_c$  and the highest value of  $\Delta T_m$ , COP, and COPR. When the cooling load is 0 W, the system yields  $T_c$  and  $\Delta T_m$  values of 20.3 °C and 24.1 °C, respectively. When the cooling load is 2 W, the system provides  $T_c$ ,  $\Delta T_m$ , COP, and COPR of 23.4 °C, 26.9 °C, 3.31 %, and 29.9 %, respectively. The results from the present study are satisfactory and will provide guidelines for using of this new type of stack in thermoacoustic refrigerators in the future.

**Acknowledgments** The authors acknowledge the National Research Council of Thailand (NRCT) for the Research and Researchers Funds for Industries (RRI), Mr. Thunyawat Chittiphalsri from Saijo Denki International Co. Ltd., the NSTDA for the Research Chair Grant, and the Thailand Science Research and Innovation (TSRI) for Fundamental Fund 2022.

**Data Availability** Data sharing not applicable to this article as no datasets were generated or analyzed during the study. We do not wish to share our data at this moment because the next step of this research is going on and would like to keep the data until the project is finished.

## Declarations

**Conflict of interests** The authors declare that they have no competing interests.

## References

1. N. Rott, Thermoacoustics. *Adv. Appl. Mech.* **20**, 135–175 (1980)
2. T.J. Hofler, Thermoacoustic refrigerator design and performance, Ph.D. Dissertation, Physics Department, University of California at San Diego, 1986.
3. G.W. Swift, Thermoacoustic engines. *J. Acoust. Soc. Am.* **84**, 1145–1180 (1988)
4. S.L. Garrett, J.A. Adef, T.J. Hofler, Thermoacoustic refrigerator for space applications. *J. Thermophys. Heat Transf.* **7**, 595–599 (1993)
5. G.W. Swift, Thermoacoustic engines and refrigerators. *Phys. Today* **48**, 22–28 (1995)
6. M. Wetzler, C. Herman, Design optimization of thermoacoustic refrigerators. *Int. J. Refrig.* **20**, 3–21 (1997)
7. J.R. Belcher, W.V. Slaton, R. Raspet, H.F. Bass, J. Lightfoot, Working gases in thermoacoustic engines. *J. Acoust. Soc. Am.* **105**, 2677–2684 (1999)
8. M.E. Poese, S.L. Garret, Performance measurements on a thermoacoustic refrigerator driven at high amplitudes. *J. Acoust. Soc. Am.* **107**, 2480–2486 (2000)
9. M.E.H. Tijani, J.C.H. Zeegers, A.T.A.M. de Waele, Construction and performance of a thermoacoustic refrigerator. *Cryogenics* **42**, 59–66 (2002)
10. M.E.H. Tijani, J.C.H. Zeegers, A.T.A.M. de Waele, Design of thermoacoustic refrigerators. *Cryogenics* **42**, 49–57 (2002)
11. C. Herman, Y. Chen, A simplified model of heat transfer in heat exchangers and stack plates of the thermoacoustic refrigerators. *Heat Mass Transfer* **42**, 901–917 (2006)
12. M. Akhavanbazaz, M.H.K. Siddiqui, R.B. Bhat, The impact of gas blockage on the performance of a thermoacoustic refrigerator. *Exper. Therm. Fluid Sci.* **32**, 231–239 (2007)
13. E.C. Nsofor, A. Ali, Experimental study on the performance of the thermoacoustic refrigerating system. *Appl. Therm. Eng.* **29**, 2672–2679 (2009)
14. S.H. Tasnim, S. Mahmud, R.A. Fraser, Effects of variation in working fluids and operating conditions on the performance of a thermoacoustic refrigerator. *Int. Commun. Heat Mass Transfer* **39**, 762–768 (2012)
15. B.R. Nayak, G. Pundarika, B. Arya, Influence of stack geometry on the performance of thermoacoustic refrigerator. *Indian Acad. Sci.* **42**, 223–230 (2017)
16. S.G. Yahya, X. Mao, A.J. Jaworski, Experimental investigation of thermal performance of random stack materials for use in standing wave thermoacoustic refrigerators. *Int. J. Refrig.* **75**, 52–63 (2017)
17. C. Wantha, The impact of stack geometry and mean pressure on cold end temperature of stack in thermoacoustic refrigeration systems. *Heat Mass Transf.* **54**, 2153–2161 (2018)
18. P. Chaiwongsa, S. Wongwises, Experimental investigation on the performance of the air-based standing wave thermoacoustic refrigerator using heat pipe as heat exchangers. *Int. J. Air Cond. Refrig.* **28**, 1–16 (2020)
19. P. Chaiwongsa, S. Wongwises, Effect of the blockage ratios of circular stack on the performance of the air-based standing wave thermoacoustic refrigerator using heat pipe, *Case Stud. Therm. Eng.* **64**, 1–13 (2021)

**Publisher's Note** Springer Nature remains neutral with regard to jurisdictional claims in published maps and institutional affiliations.